

Avalanches in CuZrAl metallic glasses

Tero Mäkinen,^{1,*} Anshul D. S. Parmar,^{2,†} Silvia Bonfanti,² and Mikko J. Alava^{1,2}

¹*Aalto University, Department of Applied Physics, P. O. Box 15600, 00076 Aalto, Espoo, Finland*

²*NOMATEN Centre of Excellence, National Center for Nuclear Research,
ul. A. Soltana 7, 05-400 Swierk/Otwock, Poland*

Metallic glasses have mechanical properties, which exhibit avalanches in the disguise of stress drops. We study these phenomena in a classical metallic glass system CuZrAl by athermal quasistatic shear and varying the element concentrations and for pure CuZr 50/50 case the cooling rate. The resulting mechanical properties are close to the behaviour found experimentally. At small strains, the pristine systems are akin to other glassy systems with a so-called gap distribution with a small positive exponent. Critical avalanching behaviour is found only approaching the yield point. The post-yield stress drops are universal, and the gap distribution becomes flat.

INTRODUCTION

Despite the no-long-range structural order, metallic glasses (MGs) exhibit elasticity to the external shear and will flow if sufficient shear stress is applied. The plasticity can be conceived as consisting of elementary rearrangements, that are localized in the so-called shear transformation zones (STZs), but display long-range elastic interactions. Below a critical strain, the events are localized [1–4] and result in crackling noise-like stress drops. The piecewise elastic response is intersected with these plastic stress drops and as one approaches the yield point, the plastic events manifest as nonlocalized avalanches, and finally, the system reaches a well-defined steady state.

As an elementary observation, the statistics of such plastic excitations correlate with the microscopic description. The probability distribution function $p(\Delta\gamma; \gamma)$ in the strain interval over accumulated strain γ , is defined by the additional shear strain $\Delta\gamma$ required to trigger an avalanche at the strain γ [5–7]. This is conceptually useful also in order to make a connection to depinning transition theory [8]. The empirical pseudogap, i.e. $\lim_{\Delta\gamma \rightarrow 0} p(\Delta\gamma; \gamma = 0^+) \propto \Delta\gamma^\theta$ is characterized by the power-law behavior of the $\Delta\gamma$ distribution at small values. The exponent θ does not claim any universality and is found to be dimension and glass preparation protocol dependent [6, 8, 9]. However, as the yield is approached from below, initially, the exponent rapidly drops and in the steady state becomes zero beyond the yield strain [7, 9, 10]. In the simplistic picture, in response to the deformation, the plastic rearrangements and their spatial and temporal correlations can be considered in the context of the pinning to depinning transition [11], making a depinning event the epicentre of an avalanche. The role of the critical threshold in the depinning against the flow and the growth of the local strain can explicitly be considered for the macroscopic yield stress and the shear band [11–13].

The studies of model glass systems by molecular dynamics extend over a long period of time with the main

questions being asked concentrating on the critical exponents of the yield transition and the effects of inertia and temperature [6, 14]. These naturally have been based on the STZ and depinning analogies and later this work has expanded to consider the effect of sample preparation or cooling. The current understanding points towards a critical point in disorder, separating systems with a finite stress drop (“good glasses”) from those with no drop (“bad glasses”) [15]. While this is indicated by mean-field arguments the properties of the steady-state beyond the yield stress and the approach to that are an open question in terms of universality, apart from the generic idea of a gap distribution, applied both below and above the yield stress.

Recently some work has been done on more realistic (metallic) glass models, including the CuZr system, including aspects like the geometric details of the yield events as plastic strain develops [16–19] with partial evidence for the avalanche statistics in general. One may confront these with generic glass criticality [15] and generally a stress drop exponent for the distribution $p(\Delta\tau)$ of stress drops $\Delta\tau$ emerges with a value of about $1.2 \dots 1.4$. As usual, the distribution is via its cutoff $\Delta\tau_0$ coupled to the value of the mean drop at a given strain, $\langle\Delta\tau\rangle$ as noted by Shang *et al.* [20]. Interestingly in the Lennard-Jones system studied there power-law like activity was found for small γ .

The CuZr(Al) system is the ubiquitous metallic glass for its good glass forming ability and the possibility of controlling its properties again by cooling but also by the composition. In particular it was recognized some time ago [21] that aluminum brings beneficial effects as it seems by forming local structural motifs to improve mechanical properties. Thus it is of interest to compare this key glass family *in silico* to expectations from glass theory and to experimental observations.

For instance, the experimental work of Das *et al.* [22] shows that the composition Cu_{47.5}Zr_{47.5}Al₅ has superior mechanical properties, such as higher strength, improved ductility, and work-hardenability, compared to the binary Cu₅₀Zr₅₀, prepared by arc melting. Same optimal 5 % Al was found by Yu & Bai [23] when considering

Composition	N	\dot{T} [K/s]	G [GPa]	τ_{\max} [GPa]	γ_{\max}
Cu _{0.50} Zr _{0.50}	6000	10 ¹¹	24.74	1.811	0.1095
Cu _{0.50} Zr _{0.50}	6000	10 ¹²	23.74	1.760	0.1035
Cu _{0.50} Zr _{0.50}	6000	10 ¹³	22.90	1.537	0.1035
Cu _{0.50} Zr _{0.50}	6000	10 ¹⁴	20.47	1.049	0.0945
Cu _{0.50} Zr _{0.50}	6000	10 ¹⁵	16.95	0.845	0.9025
Cu _{0.30} Zr _{0.70}	6000	10 ¹²	19.00	0.987	0.0945
Cu _{0.70} Zr _{0.30}	6000	10 ¹²	24.84	1.580	0.1065
Cu _{0.47} Zr _{0.47} Al _{0.06}	6000	10 ¹²	24.00	1.743	0.1005
Cu _{0.45} Zr _{0.45} Al _{0.10}	6000	10 ¹²	24.93	1.736	0.1045
Cu _{0.40} Zr _{0.40} Al _{0.20}	6000	10 ¹²	26.59	1.799	0.1095
Cu _{0.37} Zr _{0.37} Al _{0.26}	6000	10 ¹²	28.35	1.845	0.1115
Cu _{0.50} Zr _{0.50}	3000	10 ¹²	23.43	1.667	0.1025
Cu _{0.50} Zr _{0.50}	12000	10 ¹²	23.17	1.798	0.1025
Cu _{0.50} Zr _{0.50}	24000	10 ¹²	23.96	1.834	0.1045

TABLE I. Averaged mechanical parameters for the compositions used (systems of size 6000 shown in Figure 1). The columns are system size N , the cooling rate \dot{T} , the shear modulus G , the maximum shear stress τ_{\max} , and the strain corresponding to the maximum stress γ_{\max} .

maximal plastic strain and also the Poisson ratio. Furthermore, it has been shown by Pauly *et al.* [24] that addition of Al increases tensile failure stress and elastic modulus, but decreases the plastic strain. In nanoindentation experiments Poltronieri *et al.* [25] found an increase in shear and elastic moduli as well as hardness with increasing Al content (up to 12 %). Similarly, Cheung & Shek [26] in their nanoindentation experiments found increase in hardness and elastic modulus with increasing Al content (up to 10 %). Additionally they saw a decrease in creep displacement.

The structure of this paper is as follows. In the next section we briefly go through the methodology needed to study the shear response of MGs in silico. The results part is divided roughly into three themes: the generic mechanical properties and their dependence on cooling (pure CuZr) and composition, the small-strain regime before yielding, and the statistics of yielding in the steady-state after that. Finally, we finish with a summary.

METHODS

Simulation methods — Metallic glass samples are simulated using molecular dynamics methods implemented in LAMMPS [27], where the interactions are modelled through the embedded atom method (EAM) as developed by Ref. [28]. The simulations are performed in a cubic box with periodic boundary conditions in three dimensions. We vary the element concentrations, system sizes N , and cooling rates \dot{T} as reported in Tbl. I.

Hybrid molecular dynamics + Monte Carlo (MD+MC)

algorithm — To generate metallic glasses we employ a hybrid molecular dynamics + Monte Carlo (MD+MC) scheme under the variance-constrained semi-grand canonical ensemble (VC-SGC) [29]. This VC-SGC MC scheme allows exploring the configurational degrees of freedom by randomly selecting an atom and attempting to change its type, while also calculating the corresponding energy and *concentration* changes. It allows to target specific concentration ranges while maintaining a fixed total number of particles and volume. Acceptance of these transmutations follows the Metropolis criterion, ensuring the preservation of detailed balance. On the other hand, the relaxation processes are accounted for by the MD integration steps. To maintain the desired concentration within the system [29], we set the variance parameter $\kappa=10^3$. The differences in chemical potential relative to Zr using hybrid MD+MC simulations under the semi-grand canonical ensemble at a temperature of 2000 K and the specific set of parameters that minimize the composition errors in relation to the desired concentration can be found in Ref. [30]. The hybrid scheme is also used for CuZr by Ref. [31].

Quenching Protocol — The glass state is obtained through quenching in the isobaric-isothermal ensemble (NpT) from the liquid at 2000 K to 300 K using a cooling rate reported in Tbl. I and a time step $\Delta t=1$ fs. For the MD+MC scheme, every 20 MD steps, a MC cycle consisting of $N/4$ attempts is performed. The cooling process is performed by integrating the Nosé-Hoover equations with damping parameters $\tau_T=2$ fs and $\tau_p=5$ ps for the thermostat and barostat. All results are obtained keeping the external pressure $P=0$.

Athermal quasistatic shear — The shear simulations are performed for the samples cooled to $T=300$ K. The simulation box is incrementally sheared along the x -direction with respect to the y -direction by $\delta\gamma=10^{-4}$, and at each strain increment, MD simulations are performed for a duration of 1 ps. Throughout the shearing process, we record the stress-strain response, which provides a detailed stress-strain curve for analysis (see Fig. 1). From the stress-strain curves we determine the shear modulus G , by averaging the positive slopes of the stress-strain curve for the first 1 % of strain in each configuration. The maximum stress τ_{\max} and the corresponding strain γ_y (shown in Tbl. I) are then determined from the stress-strain curve averaged over all the configurations, by taking the point corresponding to the maximum stress.

The stress drops are determined by looking at the periods when the stress τ is decreasing. The drop size $\Delta\tau$ is the difference between the the point where the stress started to decrease and the point when it starts to increase again. Drops smaller than 10^{-4} GPa are discarded. The strain increments $\Delta\gamma$ are then the

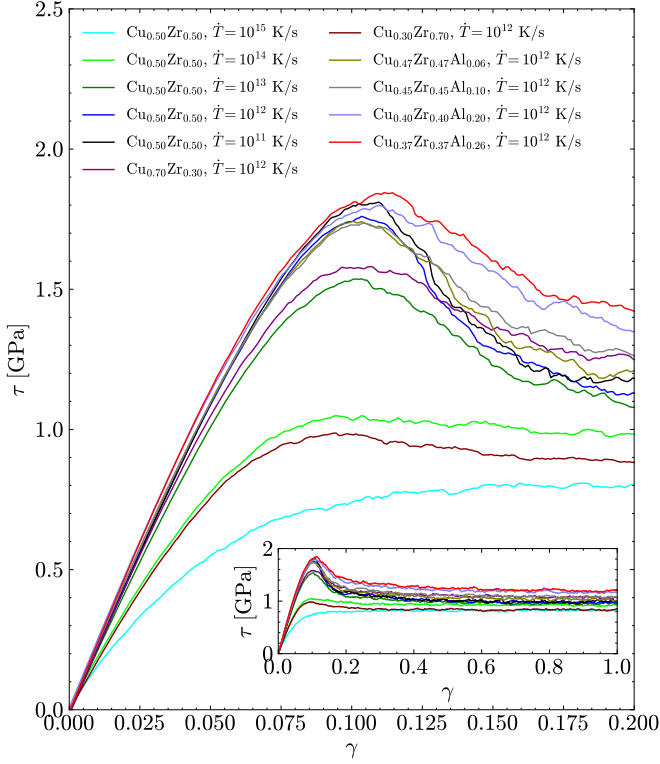


FIG. 1. The averaged stress-strain curves for various compositions and cooling rates \dot{T} (for $N=6000$). The inset shows a zoomed-out view of the same data up to $\gamma=1$, showing the steady-state behavior.

lengths of the periods between the end of a previous stress drop and the start of the subsequent drop.

Maximum likelihood fitting — The distributions observed are fitted using the maximum likelihood method [32]. For a dataset x_i (i ranging from 1 to N_x) and a probability density function $p(x; \phi_j)$, where ϕ_j are the parameters for the distribution, one computes the parameters that maximize the likelihood function $\mathcal{L}(\phi_j) = \prod_{i=1}^{N_x} p(x_i; \phi_j)$, which are the optimal parameters.

For the case of the Weibull distribution we emphasize the pseudo-gap part of the distribution, and initially do the fitting only from zero to a value $\Delta\gamma=10^{-3}$ corresponding roughly to the mode of the distribution. Fixing this estimate for the pseudo-gap exponent θ , we then fit the full distribution, using the whole dataset.

RESULTS

Generic behavior

Fig. 1 and Tbl. I show the main features of different compositions and/or cooling rates as regards the typical mechanical properties under shear. The curves of Fig. 1

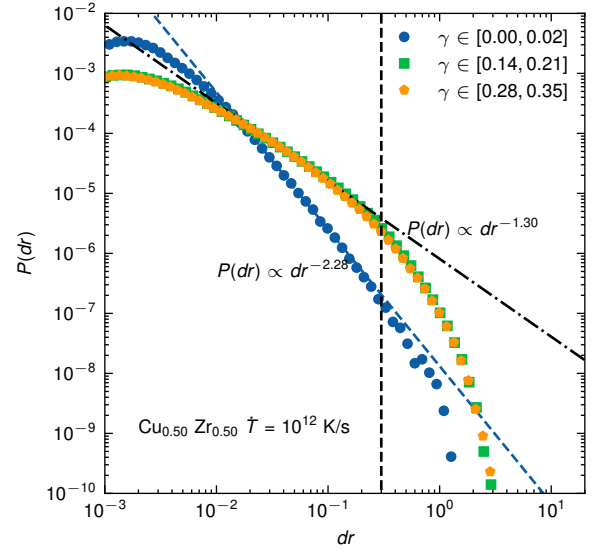


FIG. 2. Distributions of the particle's non-affine displacements at the plastic events shown in log-log scale for various strain intervals for a system of Cu₅₀Zr₅₀ with the cooling rate $\dot{T}=10^{12}$ K/s for 6000 particles. The particles are considered plastic/active if the non-affine displacement corresponds to the tails of the distribution, marked as $dr \geq 0.3$ Å [33].

(averages of 100 runs each) split roughly into two groups: ones with a pronounced stress peak (which makes it easy to define a yield stress) and ones without. The latter consists of a 30/70 CuZr mixture and two very fast-cooled 50/50 cases. The highest yield stresses are achieved with high Al contents, but the sharpest peaks with the slowest cooling rates. The Tbl. I shows the resulting mechanical characteristics with clear trends for the elastic modulus and peak/yield stress with the cooling rate and likewise a weaker but still clear trend with the addition of Al to the equiatomic CuZr composition. The results of Tbl. I for different N give some confidence limits to the values quoted, as there is a slight trend with N . The effect of Al is in agreement with the experimental picture (e.g. [25]) in that the shear modulus shows a clear but non-drastic increase with Al. Note that the change in the yield stress is in relative terms larger. After the peak, the systems enter in a flow state with the flow stress following the same order from case to case (see inset of Fig. 1).

Development of plastic deformation

Next, we consider the effects of cooling and composition with the microscopic picture of the plastic deformation. In the presence of an avalanche, the system can be viewed as the plastically deformed particles as the core and the rest of the system undergoing an elastic deformation in response to the stresses created by the imposed strain. To this end, we first estimate the particles

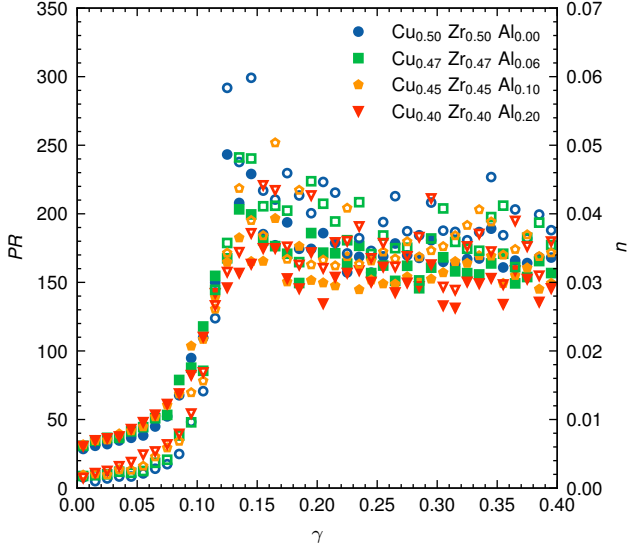


FIG. 3. For a plastic event in various compositions, the participation ratio (PR , filled symbols) and the fraction of particles in plasticity (n , open symbols) for the various concentrations of Al remains the same across the yield.

participating in a plastic deformation by considering the non-affine displacement of particles. It is observed that the distribution of single-particle displacements $p(dr)$ displays a power-law elastic profile with an exponential tail at the cutoff. The deviations from the power law account for the particles “participating” in the plastic deformations [33]. Fig. 2 shows the single-particle displacements for the plastic events in various windows of strain. The exponent of the power law, however, is found to be sensitive to the window of the strain [34]. Particles are considered “plastic” if they are displaced by more than 0.3 \AA . With this cutoff in the particle displacements, we wish to include particles that take part in the plastic deformation, and exclude particles undergoing elastic response.

The microscopic nature of the plastic deformation is defined by two different approaches. Firstly, we observe the fraction of the particles involved in the plastic response at the avalanche, i.e. $n = N_{pl}/N$, where N_{pl} is the number of particles displaced by more than the cutoff 0.3 \AA . For the second approach, we study the extent of localization of particle rearrangements resulting from the transitions between basins at the avalanches. We measure the number of involved particles in the basin’s transition to the plastic event by the participation ratio (PR), defined as

$$PR = \frac{\left[\sum_{i=1,N} dr_i^2 \right]^2}{\sum_{i=1,N} dr_i^4} \quad (1)$$

where dr_i is the displacement of particle ‘ i ’ between basins at the plastic event. In the plastic event, the PR would yield the total mobile particles involved in the

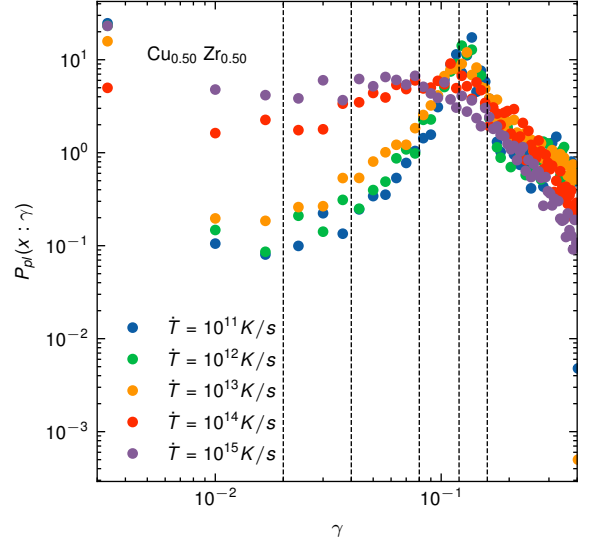


FIG. 4. The distribution of the particle undergoing the first yield event. In better annealed glasses more particles participate around the yield, which is coherent with the conventional ductile-to-brittle response. The dashed lines indicate the strains used in the snapshots in Fig. 5.

transition.

Fig. 3 shows the fraction of plastic particles and the parameter-free description of the avalanche by the participation ratio for the various concentrations of Al and the strain across the tentative yield point. The introduction of the various concentrations of Al has little effect to contribute to the deformation and does not affect the nature of the avalanches at the microscopic level.

Once established that the nature of avalanches is independent of the compositions, we further focus on the cooling rates dependent on the avalanches for the CuZr system. To discover the role of cooling in the local stability of the particles against the mechanical deformations, we record the strain for each particle for the first plastic event. Fig. 4 shows the distribution of the particle undergoing the first plastic event for the various cooling rates for the CuZr glass. The fraction of particles undergoing the first avalanche for the $\gamma \rightarrow 0$, can be found consistent with the marginal stability in the glasses [7]. In better-annealed glasses with high stability, a larger fraction of particles undergo the first plastic event in the narrow strain window near the yield. This is consistent with the increasing brittle-like response as the yield approaches. Meanwhile, the yield is gradual for poor glasses, and particles undergo the first plastic deformation across a wide range of strain values.

The question that naturally arises is “*how are the plastic events spatially distributed?*” Fig. 5 shows the spatial arrangement of the particles undergoing the first plastic event for a range of strain and cooling rates, incisively better and poorly annealed glasses. For the poor

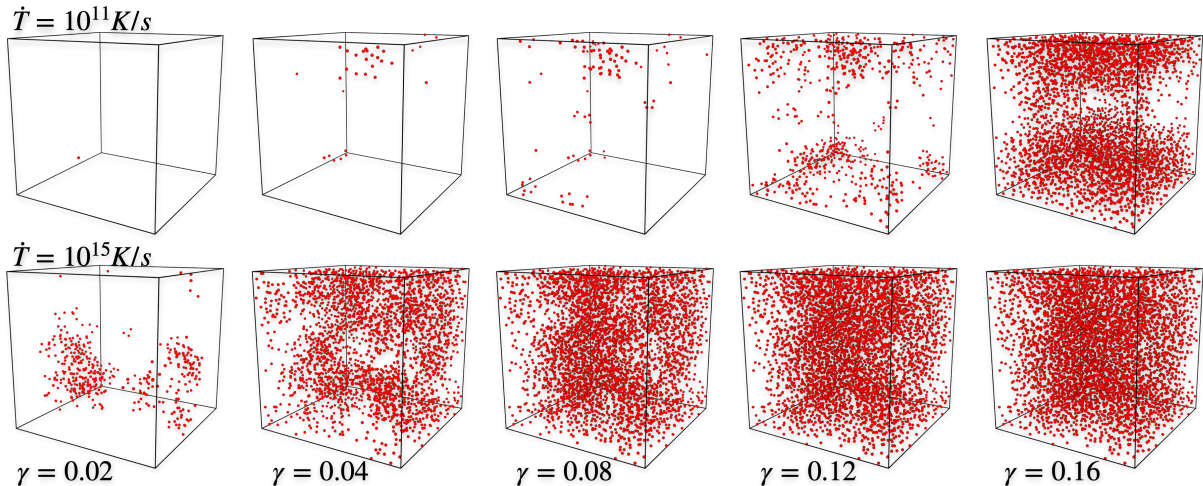


FIG. 5. The spatial profile of the particles undergone the first plastic event. Compared with the poor glass, the well-relaxed glass shows localised plastic events, which act as the nucleation points for the additional plastic events.

glass, the first plasticity for particles is observed to be strain-independent, highlighting the presence of numerous soft zones and underlying complex elastic interactions. Whereas, for the well-annealed glasses the particles undergoing the first plastic events are somewhat correlated and approach maximal around the yield, manifesting into the shear band. The overall correlation between the plastic events and cooling effect needs further attention, which we wish to address in the subsequent work with larger samples and cooling rates.

Stress drops

As discussed in the Introduction the crackling noise in the stress-strain curve is defined with the drops of stress $\Delta\tau$ and the intervals between those drops $\Delta\gamma$, giving rise to the gap distribution $p(\Delta\gamma)$.

Looking at the stress drops $\Delta\tau$ in different strain windows shows (see Fig. 6a) that they follow a power-law distribution with a Gaussian cutoff

$$p(\Delta\tau) \propto \Delta\tau^{-\beta} \exp \left[- \left(\frac{\Delta\tau}{\Delta\tau_0} \right)^2 \right] \quad (2)$$

where β is an exponent and $\Delta\tau_0$ the cutoff scale increasing with strain. Fig. 6a shows the maximum likelihood [32] fits to this distribution where over two decades of power-law scaling with an exponent of 1.16 can be observed for strain intervals after the yield point.

Even though the distribution of Eq. 2 fits the data well for all the strain bins, the power-law region is extremely small for small strains. This means that the

distributions can be fitted using a light-tailed distribution, as illustrated in the inset of Fig. 6a where stress drop distributions for the first three strain bins are plotted using a semilog scale along with an exponential fit. To quantify this we compute the Bayesian Information Criterion [35, 36]

$$\text{BIC} = -2 \ln \mathcal{L} + n_p \ln N_{\Delta\tau} \quad (3)$$

where \mathcal{L} is the likelihood function, $N_{\Delta\tau}$ the number of stress drop datapoints, and n_p the number of parameters in the chosen distribution. The lower the BIC is, the better the model fits the data. We compute the BIC for a power-law distribution with a Gaussian cutoff (Eq. 2 and $n_p=2$) and for a half-Gaussian distribution (where $n_p=1$ and $p(\Delta\tau) \propto e^{-(\Delta\tau/\Delta\tau_0)^2}$). From Fig. 6b one can see that both distributions perform roughly equally before the yield point, signifying a lack of a power-law scaling region below this point. After the yield point, the power-law fits the data significantly better.

In the steady state regime (here $\gamma > 0.50$) the stress drop distributions show completely universal behavior (see Fig. 7) for all the cooling rates and compositions. The distribution follows Eq. 2 with the same exponent $\beta=1.16$ and an universal cutoff value of $\Delta\tau_0 = 0.34$ GPa.

The behavior of the cutoff scale $\Delta\tau_0$ (see Fig. 6c) resembles the behavior seen in Figs. 3. When approaching yielding from below, the cutoff scale increases rapidly, reaching a maximum around yielding. The value then slightly decreases to a steady-state value, which is

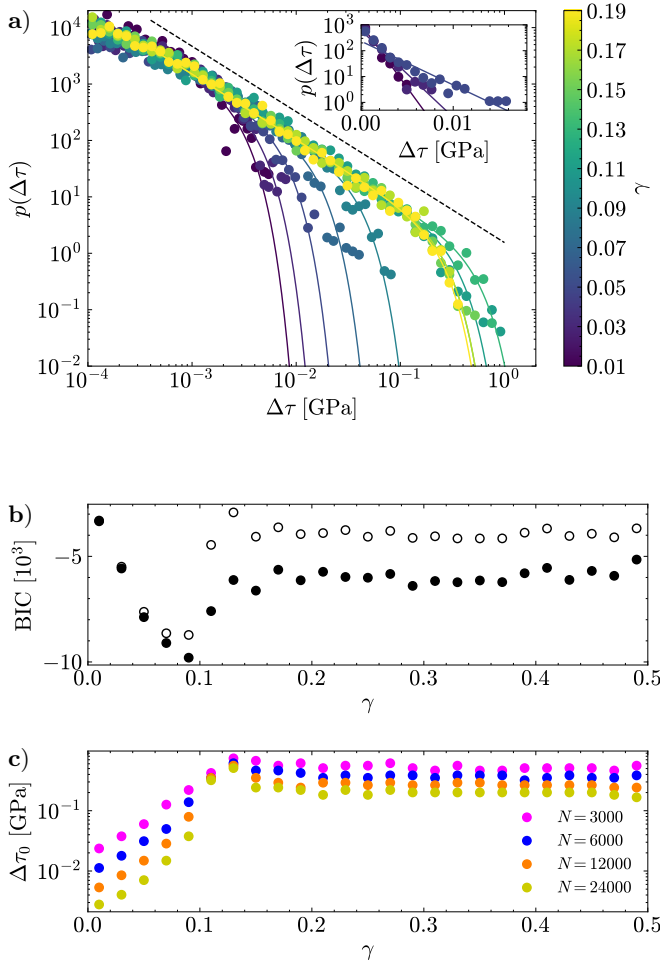


FIG. 6. **a)** The stress drop distribution (for the $\text{Cu}_{0.50}\text{Zr}_{0.50}$, $\dot{T} = 10^{12}$ K/s, $N = 24000$ system) for various strain bins indicated by the plot color. The lines are fit to Eq. 2 and the dashed black line shows the pure power-law behaviour $p(\Delta\tau) \propto \Delta\tau^{-1.16}$. The inset shows an exponential fit for the three first strain bins, showing the lack of power-law scaling. **b)** The BIC (Eq. 3) as a function of strain for the power law with Gaussian cutoff (solid dots) and the half-Gaussian distribution (hollow dots). **c)** The cutoff scale of Eq. 2 as a function of strain for different system sizes.

achieved already at around 15 % strain.

The behavior of the stress drop cutoff with the system size (Fig. 6c) shows a power-law-like scaling below the yield point, roughly system-size independent behavior at yielding, and power-law-like scaling again after yielding.

Looking at the scaling of the average stress drop with the system size (see Fig. 8a), one can see fairly robust power-law scaling $\langle \Delta\tau \rangle \propto N^{-\alpha}$. However, the exponent α changes with strain. Two distinct power-law regimes can be recognised (see Fig. 8b). At low strains, below the yield point, the average stress drop size scales with an exponent $\alpha_1 = 0.81 \pm 0.02$. At high strains, above the yield point and close to the steady-state, the exponent value of $\alpha_2 = 0.44 \pm 0.03$ can be found. Around the yield

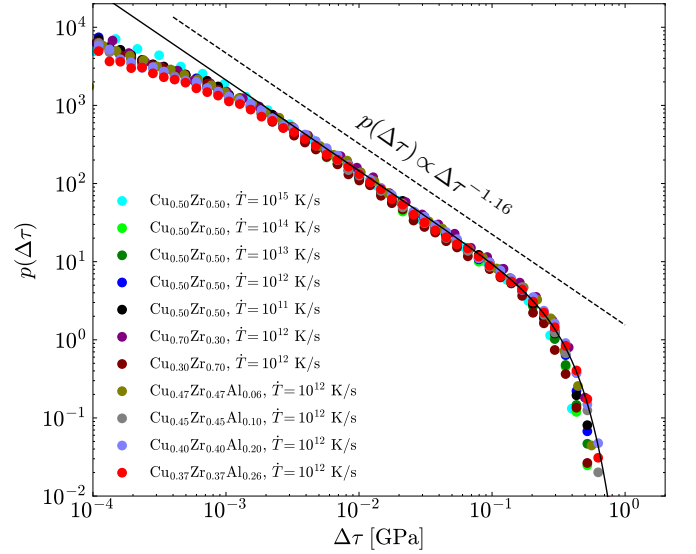


FIG. 7. The steady-state stress drop distribution for different compositions and cooling rates \dot{T} (for $N = 6000$). The solid black line corresponds to a fit to Eq. 2 which gives a universal result with cutoff $\Delta\tau_0 = 0.34$ GPa. The dashed line gives a reference power-law with the exponent $\beta = 1.16$.

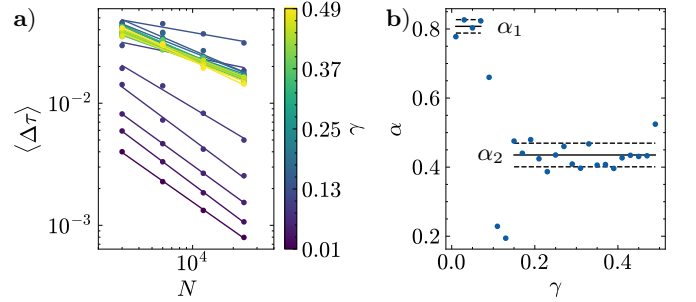


FIG. 8. **a)** The average stress drop as a function of the system size for different strain bins is illustrated by the plot colour. The lines correspond to power-law fits $\langle \Delta\tau \rangle \propto N^{-\alpha}$. **b)** The evolution of the exponent α with the strain. The black lines illustrate the exponent (solid line) and the standard deviation (dashed lines) for the pre-yield ($\alpha_1 = 0.81 \pm 0.02$) and steady-state regimes ($\alpha_2 = 0.44 \pm 0.03$).

point, the scaling vanishes as the exponent α goes close to zero. For the distribution of Eq. 2 the average value scales approximately as $\langle \Delta\tau \rangle \propto \Delta\tau_0^{1-\beta}$ which is clearly seen in the similar behavior of Figs. 6c and 8. When one accounts for the difference in definitions of the average avalanche size (multiplication by a factor N), these exponent values roughly match the results obtained in previous studies [5–7, 20].

Gap distribution

To characterize the behavior of the pseudogap, we have fitted the gap distribution using the Weibull distribu-

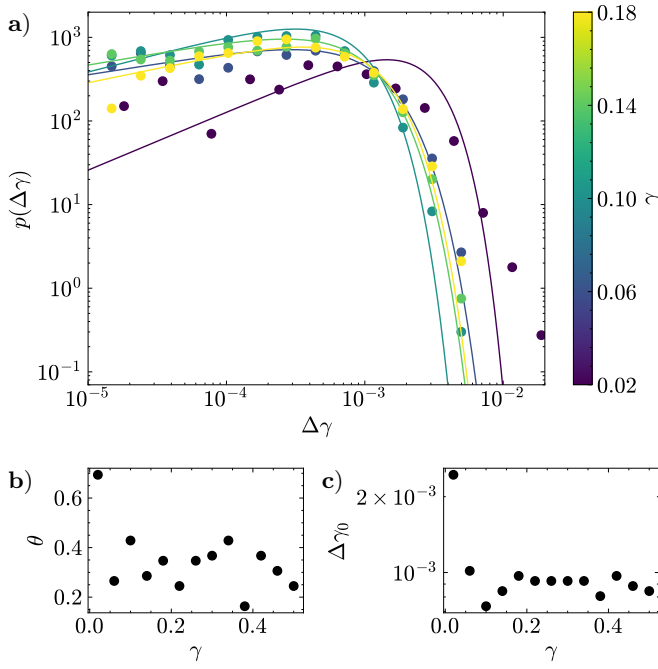


FIG. 9. **a)** The gap distribution or the strain interval distribution (for $\text{Cu}_{0.50}\text{Zr}_{0.50}$, $\dot{T} = 10^{11}$ K/s, $N = 24000$) for various strain bins indicated by the plot color. The lines are fits to Eq. 4. **b)** The exponent of Eq. 4 as a function of the strain. **c)** The cutoff scale of Eq. 4 as a function of the strain.

tion (see Fig. 9a)

$$p(\Delta\gamma) \propto \Delta\gamma^\theta \exp \left[- \left(\frac{\Delta\gamma}{\Delta\gamma_0} \right)^{1+\theta} \right] \quad (4)$$

where θ corresponds to the gap exponent and $\Delta\gamma_0$ to the cutoff scale.

The values of the gap exponent start (at low strains) close to $\theta = 0.7$ and rapidly decrease to values around $\theta = 0.3 \pm 0.1$ (see Fig. 9b). The cutoff scale $\Delta\gamma_0$ also starts from a high value, decreases to a minimum value around yielding, and then increases to a steady-state value (see Fig. 9c), mirroring the behavior of the stress drop cut-off $\Delta\tau_0$.

It is noteworthy that the tail of the distribution in the first strain bin does not follow the Weibull distribution very well. Instead, it shows a much wider tail, extending to half of a decade higher values than the distributions of the other strain bins.

Fig. 10 finally shows in the post-yield regime how the drop rate and "stress production rate" (binned sum of stress drops) scales with $\Delta\gamma$. For very small strain increments the rates are low and constant in agreement with the trivial assumption of what follows from the gap distribution in this limit. Beyond a strain of about 10^{-3} both rates start to increase apparently linearly to approach the average event and stress drop rates.

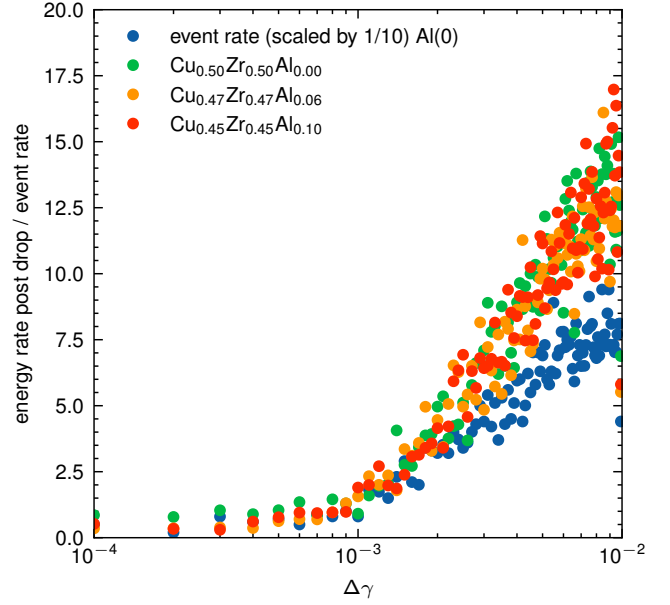


FIG. 10. Post-stress drop correlations in the steady-state flow: event rate, and the stress drop rate for systems with different Al contents.

CONCLUSIONS

The modelling studies of metallic glasses have not tried much to handshake with the general theory of glass mechanical properties. Here we have taken a look at the typical CuZrAl system under athermal quasistatic shear conditions regarding the early strain part, the typical mechanical properties and the steady-state flow beyond the yield point.

The impact of composition and cooling rate are found to be as expected as regards the impact on elastic modulus and yield stress. The development of plastic deformation shows some interesting differences as regards the impact of "how good the glass is" (cooling) but again adding more and more Aluminium shows that the composition has little effect in that all the species contribute to the deformation.

The statistics of stress drops exhibit some differences from previous studies. The early time response is typical of virgin disordered systems with a positive gap exponent. However, avalanches are not really common until strains of a substantial fraction of the yield strain are reached. The steady-state flow is found to be entertainingly superuniversal in that for all the (many) cases studied here we find the same exponent, roughly in line with earlier works, and the same cut-off. This prediction would be interesting to test in experiments.

ACKNOWLEDGMENTS

T.M. and M.J.A. acknowledge the support from FinnCERES flagship (grant no. 151830423), Business Finland (grant nos. 211835, 211909, and 211989), and Future Makers programs. M.J.A. acknowledges support from the Academy of Finland Center of Excellence program (program nos. 278367 and 317464), as well as the Finnish Cultural Foundation. A.D.S.P, S.B. and M.J.A. acknowledge support from the European Union Horizon 2020 research and innovation program under Grant Agreement No. 857470 and the European Regional Development Fund via the Foundation for Polish Science International Research Agenda PLUS program under Grant No. MAB PLUS/2018/8. S.B. acknowledges support through SONATABIS grant DEC-2023/50/E/ST3/00569 from the National Science Center in Poland. The authors acknowledge the computational resources provided by the Aalto University School of Science “Science-IT” project.

* tero.j.makinen@aalto.fi

† Anshul.Parmar@ncbj.gov.pl

- [1] AS Argon. Plastic deformation in metallic glasses. *Acta metallurgica*, 27(1):47–58, 1979.
- [2] Michael L Falk and James S Langer. Dynamics of viscoplastic deformation in amorphous solids. *Physical Review E*, 57(6):7192, 1998.
- [3] Anne Tanguy, Fabien Leonforte, and J L Barrat. Plastic response of a 2D Lennard-Jones amorphous solid: Detailed analysis of the local rearrangements at very slow strain rate. *The European Physical Journal E*, 20:355–364, 2006.
- [4] Brani Lin Li, Eric R Homer, and Christopher A Schuh. Shear transformation zone dynamics model for metallic glasses incorporating free volume as a state variable. *Acta materialia*, 61(9):3347–3359, 2013.
- [5] Anaël Lemaitre and Christiane Caroli. Plastic response of a 2d amorphous solid to quasi-static shear: Ii-dynamical noise and avalanches in a mean field model. *arXiv preprint arXiv:0705.3122*, 2007.
- [6] Smarajit Karmakar, Edan Lerner, and Itamar Procaccia. Statistical physics of the yielding transition in amorphous solids. *Physical Review E—Statistical, Nonlinear, and Soft Matter Physics*, 82(5):055103, 2010.
- [7] HGE Hentschel, Prabhat K Jaiswal, Itamar Procaccia, and Srikanth Sastry. Stochastic approach to plasticity and yield in amorphous solids. *Physical Review E*, 92(6):062302, 2015.
- [8] Jie Lin, Edan Lerner, Alberto Rosso, and Matthieu Wyart. Scaling description of the yielding transition in soft amorphous solids at zero temperature. *Proceedings of the National Academy of Sciences*, 111(40):14382–14387, 2014.
- [9] Jie Lin, Thomas Gueudré, Alberto Rosso, and Matthieu Wyart. Criticality in the approach to failure in amorphous solids. *Physical review letters*, 115(16):168001, 2015.
- [10] Jie Lin and Matthieu Wyart. Mean-field description of plastic flow in amorphous solids. *Physical review X*, 6(1):011005, 2016.
- [11] Jean-Christophe Baret, Damien Vandembroucq, and Stéphane Roux. Extremal model for amorphous media plasticity. *Physical review letters*, 89(19):195506, 2002.
- [12] Alexandre Nicolas, Ezequiel E Ferrero, Kirsten Martens, and Jean-Louis Barrat. Deformation and flow of amorphous solids: Insights from elastoplastic models. *Reviews of Modern Physics*, 90(4):045006, 2018.
- [13] Alberto Rosso, James P Sethna, and Matthieu Wyart. Avalanches and deformation in glasses and disordered systems. *arXiv preprint arXiv:2208.04090*, 2022.
- [14] K. Michael Salerno and Mark O. Robbins. Effect of inertia on sheared disordered solids: Critical scaling of avalanches in two and three dimensions. *Phys. Rev. E*, 88:062206, Dec 2013.
- [15] Misaki Ozawa, Ludovic Berthier, Giulio Biroli, Alberto Rosso, and Gilles Tarjus. Random critical point separates brittle and ductile yielding transitions in amorphous materials. *Proceedings of the National Academy of Sciences*, 115:6656–6661, 2018.
- [16] BA Sun, HB Yu, W Jiao, HY Bai, DQ Zhao, and WH Wang. Plasticity of ductile metallic glasses: a self-organized critical state. *Physical review letters*, 105(3):035501, 2010.
- [17] Tomoaki Niiyama, Masato Wakeda, Tomotsugu Shimokawa, and Shigenobu Ogata. Structural relaxation affecting shear-transformation avalanches in metallic glasses. *Physical Review E*, 100(4):043002, 2019.
- [18] Shiheng Cui, Huashan Liu, and Hailong Peng. Anisotropic correlations of plasticity on the yielding of metallic glasses. *Physical Review E*, 106(1):014607, 2022.
- [19] Alexandra Lagogianni, Chen Liu, Kirsten Martens, and Konrad Samwer. Plastic avalanches in the so-called elastic regime of metallic glasses. *European Physical Journal B*, 91:104, 2018.
- [20] Baoshuang Shang, Pengfei Guan, and Jean-Louis Barrat. Elastic avalanches reveal marginal behavior in amorphous solids. *Proceedings of the National Academy of Sciences*, 117(1):86–92, 2020.
- [21] Akihisa Inoue and Wei Zhang. Formation, thermal stability and mechanical properties of cu-zr-al bulk glassy alloys. *Materials Transactions*, 43(11):2921–2925, 2002.
- [22] Jayanta Das, Mei Bo Tang, Ki Buem Kim, Ralf Theissmann, Falko Baier, Wei Hua Wang, and Jürgen Eckert. “work-hardenable” ductile bulk metallic glass. *Physical review letters*, 94(20):205501, 2005.
- [23] Peng Yu and HY Bai. Poisson’s ratio and plasticity in CuZrAl bulk metallic glasses. *Materials Science and Engineering: A*, 485(1-2):1–4, 2008.
- [24] S Pauly, S Gorantla, G Wang, U Kühn, and J Eckert. Transformation-mediated ductility in cuzr-based bulk metallic glasses. *Nature materials*, 9(6):473–477, 2010.
- [25] C. Poltronieri, A. Brognara, F. Bignoli, S. Evertz, P. Djemia, D. Faurie, F. Challali, C.H. Li, L. Belliard, G. Dehm, J.P. Best, and M. Ghidelli. Mechanical properties and thermal stability of ZrCuAl_x thin film metallic glasses: Experiments and first-principle calculations. *Acta Materialia*, 258:119226, 2023.
- [26] TL Cheung and CH Shek. Thermal and mechanical properties of cu–zr–al bulk metallic glasses. *Journal of Alloys*

- and Compounds*, 434:71–74, 2007.
- [27] S. Plimpton, P. Crozier, and A. Thompson. LAMMPS—large-scale atomic/molecular massively parallel simulator. *Sandia National Laboratories*, 18:43, 2007.
 - [28] YQ Cheng, E Ma, and HW Sheng. Atomic level structure in multicomponent bulk metallic glass. *Physical Review Letters*, 102(24):245501, 2009.
 - [29] Babak Sadigh, Paul Erhart, Alexander Stukowski, Alfredo Caro, Enrique Martinez, and Luis Zepeda-Ruiz. Scalable parallel Monte Carlo algorithm for atomistic simulations of precipitation in alloys. *Physical Review B*, 85(18):184203, 2012.
 - [30] Rene Alvarez-Donado, Silvia Bonfanti, and Mikko Alava. Simulated multi-component metallic glasses akin to experiments. *arXiv preprint [arXiv:2309.05806](https://arxiv.org/abs/2309.05806)*, 2023.
 - [31] Zhen Zhang, Jun Ding, and Evan Ma. Shear transformations in metallic glasses without excessive and predefinable defects. *Proceedings of the National Academy of Sciences*, 119(48):e2213941119, 2022.
 - [32] Jordi Baró and Eduard Vives. Analysis of power-law exponents by maximum-likelihood maps. *Physical Review E*, 85(6):066121, 2012.
 - [33] Thomas B Schröder, Srikanth Sastry, Jeppe C Dyre, and Sharon C Glotzer. Crossover to potential energy landscape dominated dynamics in a model glass-forming liquid. *The Journal of Chemical Physics*, 112(22):9834–9840, 2000.
 - [34] Premkumar Leishangthem, Anshul DS Parmar, and Srikanth Sastry. The yielding transition in amorphous solids under oscillatory shear deformation. *Nature communications*, 8(1):14653, 2017.
 - [35] Thomas Leonard and John SJ Hsu. *Bayesian methods: an analysis for statisticians and interdisciplinary researchers*, volume 5. Cambridge University Press, 2001.
 - [36] Tero Mäkinen, Jérôme Weiss, David Amitrano, and Philippe Roux. History effects in the creep of a disordered brittle material. *Physical Review Materials*, 7(3):033602, 2023.